3D Printed Optical Quality Silica and Silica–Titania Glasses from Sol–Gel Feedstocks

*Joel F. Destino, Nikola A. Dudukovic, Michael A. Johnson, Du T. Nguyen, Timothy D. Yee, Garth C. Egan, April M. Sawvel, William A. Steele, Theodore F. Baumann, Eric B. Duoss, Tayyab Suratwala, and Rebecca Dylla-Spears**

A method for fabricating optical quality silica and silica–titania glasses by three-dimensional (3D) printing is reported. Key to this success is the combination of sol–gel derived silica and silica–titania colloidal feedstocks, direct ink writing (DIW) technology, and conventional glass thermal processing methods. Printable silica and silica–titania sol inks are prepared directly from molecular precursors by a simple one-pot method, which is optimized to yield viscous, shear-thinning colloidal suspensions with tuned rheology ideal for DIW. After printing, the parts are dried and sintered under optimized thermal conditions to ensure complete organic removal and uniform densification without crystallization. Characterizations of the 3D-printed pure silica and silica–titania glasses show that they are equivalent to commercial optical fused silica and silica–titania glasses. More specifically, they exhibit comparable chemical composition, SiO_2 network structure, refractive index, dispersion, optical transmission, and coefficient of thermal expansion. 3D-printed silica and silica–titania glasses also exhibit comparable polished surface roughness and meet refractive index homogeneity standards within range of commercial optical grade glasses. This method establishes 3D printing as a viable tool to create optical glasses with compositional and geometric configurations that are inaccessible by conventional optical fabrication methods.

1. Introduction

The chemical composition of a glass directly affects its optical, thermal, and mechanical properties. As a consequence, a multitude of glass compositions are commercially available to serve different applications.[1,2] For example, high quality fused silica glass is a desirable optical material because it exhibits broadband transparency (UV–visible–near infrared (NIR)), is chemically resistant and thermally stable, and is readily polished to a high quality finish. Addition of titania to silica glass (≈7.5 wt%) has been shown to reduce thermal expansion and increase the refractive index. As a result, silica–titania glasses have been developed extensively as ultralow expansion (ULE) materials[3] and pursued for fabricating optical components such as mirrors, waveguides,[4,5] and gradient index glass optics.[6] Commercial glasses are typically formed by melting together the constituent materials in proper proportions and with sufficient uniformity to meet stringent optical homogeneity standards.

The development of additive manufacturing methods for biomaterials, ceramics, polymers, and metals have enabled researchers to explore design of components that cannot be accessed through alternative fabrication methods.[7–13] Although several methods for 3D printing of transparent glass have been explored, none have yet created glass of sufficient quality to compete with conventionally produced glasses for optical applications. For example, binder jetting, laser melting, and glass powder sintering techniques yield opaque, porous glass and would require additional tuning to achieve transparent silica glass.[14] Transparent glass has been printed via fused deposition and filament feed methods, which melt glass stock by direct heating or under CO_2 laser irradiation.[15–17] However, uncontrolled thermal gradients present during melting and printing may compromise the achievable bulk refractive index homogeneity of the printed parts, and bubbles can easily be trapped between the high viscosity filaments. In a different approach, a fumed silica-loaded, photocurable polymer is photolithographically printed into complex shapes and thermally treated afterward to form a fully dense, transparent glass.[18,19] This technique is promising, but it may not be easily adapted for fabrication of more complex glasses with compositional profiles. Additionally, lithography leaves behind characteristic axial layer demarcations at the build-face, and bulk optical characterization beyond UV–vis transmission measurements have not yet been demonstrated.

Prof. J. F. Destino
Chemistry Department
Creighton University
Omaha, NE 68178, USA

Dr. N. A. Dudukovic, Dr. M. A. Johnson, Dr. D. T. Nguyen, T. D. Yee, Dr. G. C. Egan, Dr. A. M. Sawvel, W. A. Steele, Dr. T. F. Baumann, Dr. E. B. Duoss, Dr. T. Suratwala, Dr. R. Dylla-Spears
Lawrence Livermore National Laboratory
P.O. Box 808, Livermore, CA 94551, USA
E-mail: dyllaspears1@llnl.gov

The ORCID identification number(s) for the author(s) of this article can be found under https://doi.org/10.1002/admt.201700323.

DOI: 10.1002/admt.201700323

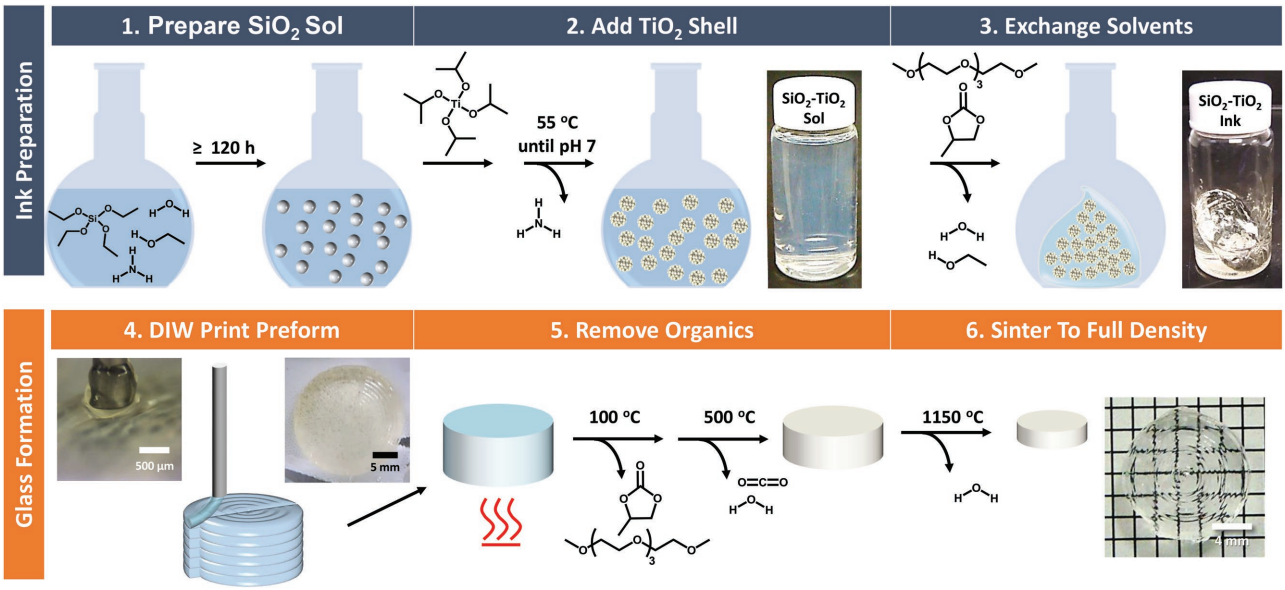

Figure 1. Sol–gel derived DIW SiO_2/SiO_2–TiO_2 glass fabrication scheme. (1) SiO_2 particle sol preparation. (2) TiO_2–SiO_2 core–shell particle preparation. (3) Ink preparation via solvent exchange from particle sol to DIW printable ink. (4) DIW printing of glass preform. (5) Organic removal to low density inorganic glass preform. (6) Sintering to full density optical quality glass (unpolished).

Recently, our group demonstrated a direct ink writing (DIW) approach to prepare transparent fused silica glass.[20] In DIW, 3D objects are prepared through filament-by-filament assembly of a shear-thinning ink, which is extruded through a nozzle in a programed pattern. Upon exiting the nozzle, the ink solidifies through a structure-building process (i.e., a chemical reaction, evaporation, gelation, or temperature-induced phase change). In the case of DIW silica inks, the ink is a suspension of fumed silica in organic solvent. After the ink is printed into a desired 3D object, the printed part is thermally treated to remove the organic components and sintered to a fully dense, transparent, crack-free glass. Multicomponent feedstocks are easily adapted to DIW by programing additional inks to extrude through a single shared nozzle or several independent nozzles.[21] One drawback of our past work, and the work of others,[18] is a reliance on commercial fumed silica feedstocks. Fumed silica materials contain adsorbed water and organic contaminants, and they are notoriously agglomerated, polydisperse, as well as hazardous and challenging to handle.[22,23] In addition, dependence on fumed silica limits the potential for chemical tuning of the glass composition to alter its material properties. Thus, fumed silica is an undesirable feedstock for additive manufacturing bona fide optical quality glasses.

Sol–gel materials are an attractive DIW feedstock for fabricating optical quality glass and have been demonstrated for printing of functional oxides.[24] Sol–gel chemistry is easily tunable and provides complete control of feedstock purity, particle composition, morphology, size, and polydispersity.[25,26] Furthermore, there is an existing wealth of knowledge of sol–gel materials in optical applications, from coatings to monolithic optics.[27–30] In this work, we report the fabrication of homogeneous, optical quality silica and silica–titania glass monoliths by DIW from one-pot, sol–gel derived feedstocks. This method demonstrates the potential of sol–gel chemistry for creating alternate glass compositions for optical 3D printing applications, which may lead to functional chemical and structural tuning of optical components.

2. Results and Discussion

2.1. Fabrication of DIW Glass and Sol–Gel Feedstocks

A convenient one-pot preparation method was developed to take silica- and titania-containing molecular components from the solution phase directly to high viscosity particle-based slurries, or inks, that can be printed by DIW. Because the particles are formed directly from molecular precursors, careful control over process chemistry and purity can be exacted. In addition, the evaporative exchange of solvents allows particles to remain dispersed during concentration and reduces the potential for contamination and problematic agglomeration. As shown in **Figure 1**, the process is only six steps and can be divided into two halves, ink preparation and DIW printed glass formation, respectively.

2.1.1. Ink Formulation and Preparation

First, SiO_2 particles are prepared by the Stöber process by mixing tetraethylorthosilicate (TEOS), water, and ammonia catalyst in an ethanol (EtOH) solvent. Particles used in this work grow to steady state in ≈5 d and are 23.6 ± 0.7 nm in diameter by dynamic light scattering (DLS), shown in **Figure 2**a. Particle size and spherical morphology were confirmed by transmission electron microscope (TEM), and are shown in Figure 2b. Larger SiO_2 particles (d ≈ 50–200 nm) were also explored, but had too little surface area to achieve an appreciable TiO_2 loading

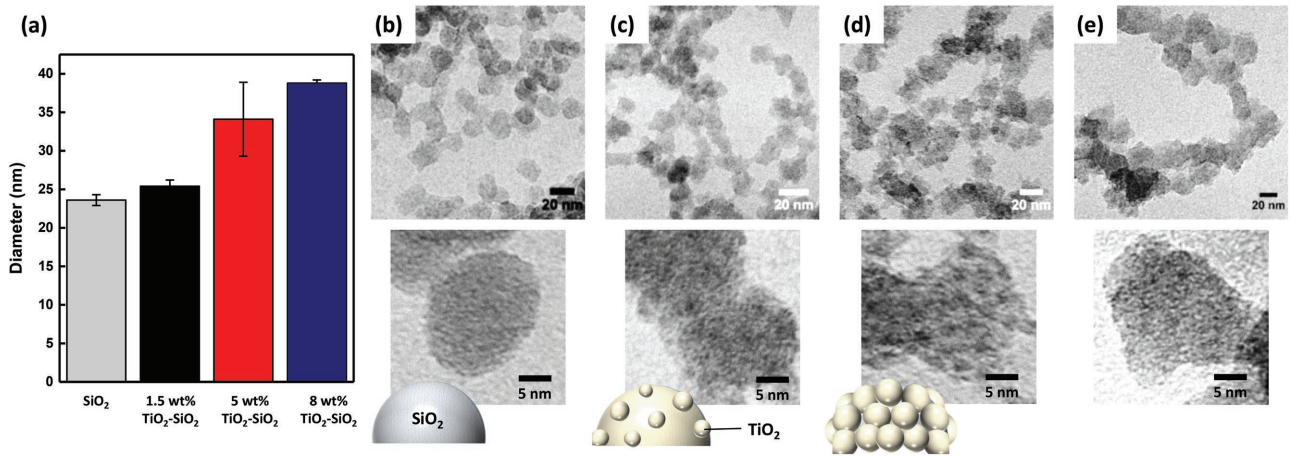

Figure 2. Determination of sol–gel SiO_2 and core–shell SiO_2–TiO_2 nanoparticle size and morphology. a) Mean diameters (±1 σ) for SiO_2, 1.5, 5, and 8 wt% TiO_2 nanoparticles determined by DLS. Transmission electron images of b) SiO_2; c) 1.5 wt%; d) 5 wt%; and e) 8 wt% TiO_2 nanoparticles.

when preparing core–shell SiO_2–TiO_2 particles. Second, for SiO_2–TiO_2 core–shell nanoparticles, titanium (IV) isopropoxide (TIP) is added to the aged SiO_2 sol and heated at 55 °C to control the reaction through evaporation of the ammonia catalyst, yielding raspberry-like particles.[31,32] Resulting nanoparticles are 25.4 ± 0.4 and 34.1 ± 4.8 nm in diameter for 1.5 and 5 wt% TiO_2-containing nanoparticles by DLS, shown in Figure 2a. TEM images shown in Figure 2c,d confirm the respective nanoparticle sizes and evolution of the raspberry-like particle morphology. The schematics below the respective images depict the relative extents of TiO_2 coatings for 1.5 and 5 wt% TiO_2–SiO_2 nanoparticles. Figure 2e shows that at 8 wt% TiO_2 loading, the SiO_2–TiO_2 nanoparticles do not clearly form in a raspberry morphology. However, DLS measurements show that the particles are typically 38.8 ± 0.5 nm, suggestive of a larger TiO_2 shell. Third, to prepare the glass ink, the high boiling point ink solvents propylene carbonate (PC) and tetraethylene glycol dimethyl ether (TG) are added to the desired sol, and then water and ethanol are removed. PC and TG are desirable solvents because they have been shown to form high solid loading, viscous shear-thinning silica suspensions.[20,33] These polar aprotic solvents provide sufficient dipole–dipole interaction with polar and charged surface groups of the SiO_2 and SiO_2–TiO_2 colloids to form stable suspensions. For SiO_2 ink, additional polar protic dispersants, 2-[2-(2-methoxyethoxy)ethoxy]acetic acid (MEEAA) and 1-hexanol, are added to improve stability (pot life) by preventing agglomeration and deterring irreversible gelation.[33] For all inks, the PC:TG ratio was optimized for pot life, reproducibility, and tuned rheology with DIW in mind. The optimized SiO_2 inks are stable on the order of one week, and the SiO_2–TiO_2 inks are stable on the order of several months in a sealed container.

The rheological behaviors of the SiO_2 and 1.5, 5, and 8 wt% TiO_2 inks are shown in **Figure 3**. All inks were formulated with matching volumetric solid loading (20 vol%) to ensure similar flow properties during printing and equal volumetric shrinkage during thermal processing. All SiO_2–TiO_2 inks exhibit pronounced shear-thinning behavior and very closely matched viscosities over a wide range of shear rates (Figure 3a). At rest, the material behaves as a viscoelastic solid (gel). At a sufficiently high shear stress (yield stress), indicated by the crossover point between the elastic and viscous moduli (Figure 3b,c), the breakdown of the particle network will result in flow. Upon cessation of high shear, the material experiences a rapid elastic recovery (Figure 3c). During printing, this fast resolidification allows for the extruded filament to retain its shape after exiting the nozzle. The rebuilding of the particle network is sufficiently quick to ensure that no hysteresis occurs during the printing process (Figure 3d), indicating strong interparticle attractions. The well-matched viscosity, elasticity, yield stress, and recovery of all four SiO_2–TiO_2 inks offer excellent potential for multimaterial printing, allowing easy alternating between inks and mixing multiple inks without affecting the overall flow properties.

The sol–gel route to printable ink feedstocks offers ink formulators a new degree of rheological control that is not achievable with formulations relying solely on commercially available feedstocks. Chemical and electrostatic environments around particles are known to contribute significantly to the observed suspension rheology.[34] In particular, it has been shown that adjusting pH or mixing particles of different compositions can shift fumed metal oxide suspension viscosities by multiple orders of magnitude and may alter or completely eliminate the yield stress.[35] As such, attempts to add either molecular species or particles of different compositions to fumed silica-based inks to alter the final glass composition are expected to have significant impact on the viscosity and yield stress. In contrast, the sol–gel inks reported here have matched rheology across multiple compositions at fixed solid loading. Furthermore, in addition to control over the particle chemistry, the sol–gel route to printable inks provides a means to control the size, texture, and polydispersity of the particles. This is crucial because mean particle size, particle size distribution, and particle morphology all strongly influence the rheology of colloidal suspensions.[34] Thus, this new method provides multiple avenues by which to tune the suspension rheology, which will improve printing process control as well as facilitate the printing of composite or gradient composition parts.

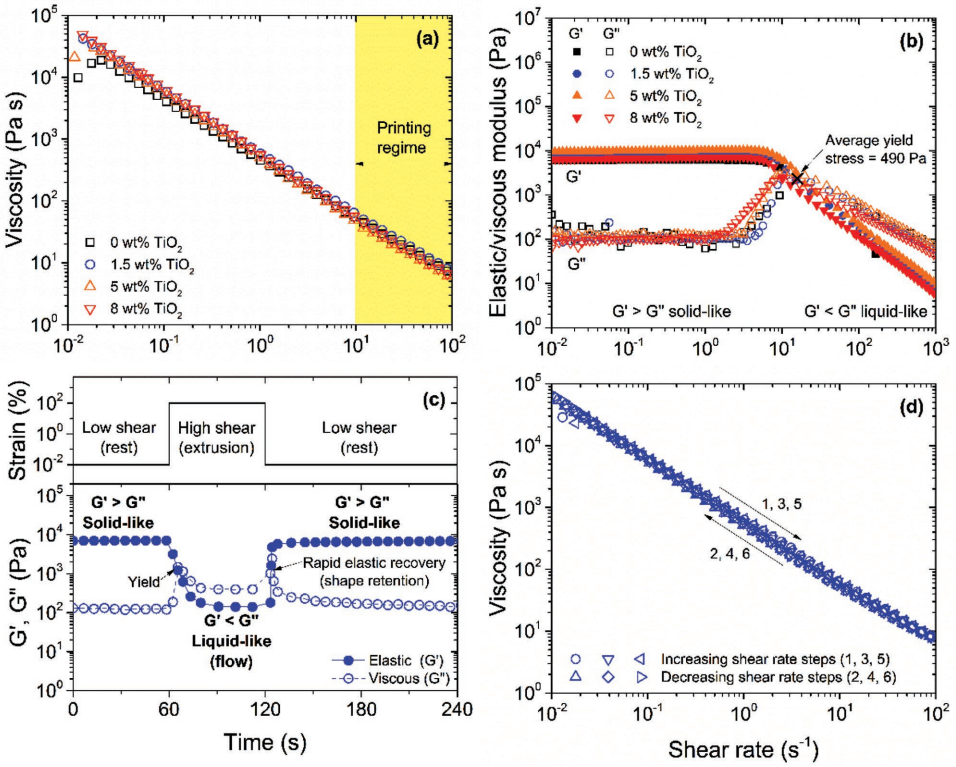

Figure 3. a) Rheological flow curves of SiO_2–TiO_2 inks under steady shear. The shear-thinning behavior and viscosities of the inks are very closely matched, allowing the same printing conditions to be used when switching between or mixing inks in multimaterial printing without changing the rheological behavior. b) Viscoelastic properties of SiO_2–TiO_2 inks from oscillatory rheological measurements. All inks exhibit almost identical elastic and viscous moduli at rest, as well as a closely matched yield stress at which liquid-like behavior (flow) can be observed. c) Elastic recovery of 1.5% TiO_2 ink. The material behaves as a gel at rest (low shear) and as a liquid at high shear. Upon cessation of high shear (flow), the ink exhibits a rapid elastic recovery, allowing for excellent filament shape retention upon extrusion from the nozzle. d) Thixotropy hysteresis of 1.5% TiO_2 ink. As the shear rate is cycled (ramping up and down consecutively), the viscosity profile remains unchanged, indicating that the particle network is restructuring at a fast rate.

2.1.2. DIW-Printed Glass Fabrication

The lower half of Figure 1 describes the fabrication of the glass structures by DIW. A viscous SiO_2 or SiO_2–TiO_2 ink is printed by DIW into a monolithic, cylindrical form of uniform composition. The low-density preforms are then slowly dried and baked, allowing for complete removal of organic species. Finally, the organic-free preforms are sintered to a fully dense glass. Optimizing the thermal processing is key to allow for complete removal of organic components, uniform shrinkage, and formation of crack-free monolithic glass structures. Figure S1 (Supporting Information) provides additional information regarding the thermal processing procedure. **Figure** 4a,b shows the evolution of DIW-printed ink preforms to fully dense SiO_2 and 1.5 wt% TiO_2 glasses, respectively. Both inks are transparent with a yellow tinge; however, the coloration is more noticeable in the TiO_2-containing inks. This color results from the organic ink components (PC, TG, etc.) as well as the Ti-alkoxide. After 5 d drying at 100 °C, the printed parts reduce in size by nearly 40 vol%. The SiO_2 part still has a yellow tinge and the 1.5 wt% TiO_2 part has a dark orange or amber coloration. This is common for TiO_2 from Ti-alkoxide precursors, and is attributed to a change in electronic structure from residual organics interacting with surface Ti sites.[36] After burnout at 500 °C, the parts undergo complete organic removal, appear colorless, and shrink by an additional 10 vol%. After sintering to 1150 °C, the parts achieve full density, reducing an additional 30 vol%, and are fully transparent. The spiral pattern visible in Figure 4a,b is the result of surface texture remaining from the final printed layer. This surface topography can be fully removed by polishing the sample, which leads to uniformly thick samples with no evident spiral pattern. As evidence, Figure 4c contains photographs of polished, fully dense, transparent SiO_2, 1.5, 5, and 8 wt% TiO_2 glasses fabricated via DIW.

2.2. Chemical and Structural Evolution

A traditional sol–gel or ceramics thermal processing procedure was developed to transform printable inks into full density glasses. Key to developing that profile is balancing the competition between structural network formation and complete removal of organics and surface groups. **Figure 5** shows the chemical and structural evolution of sol–gel nanoparticles and printed materials during thermal processing to full density. Fourier transform infrared (FTIR) spectroscopy of the dried and burned out feedstocks is used to determine the chemical evolution of the SiO_2 and SiO_2–TiO_2 nanoparticles during network formation in the early heat treatment stages. Powder

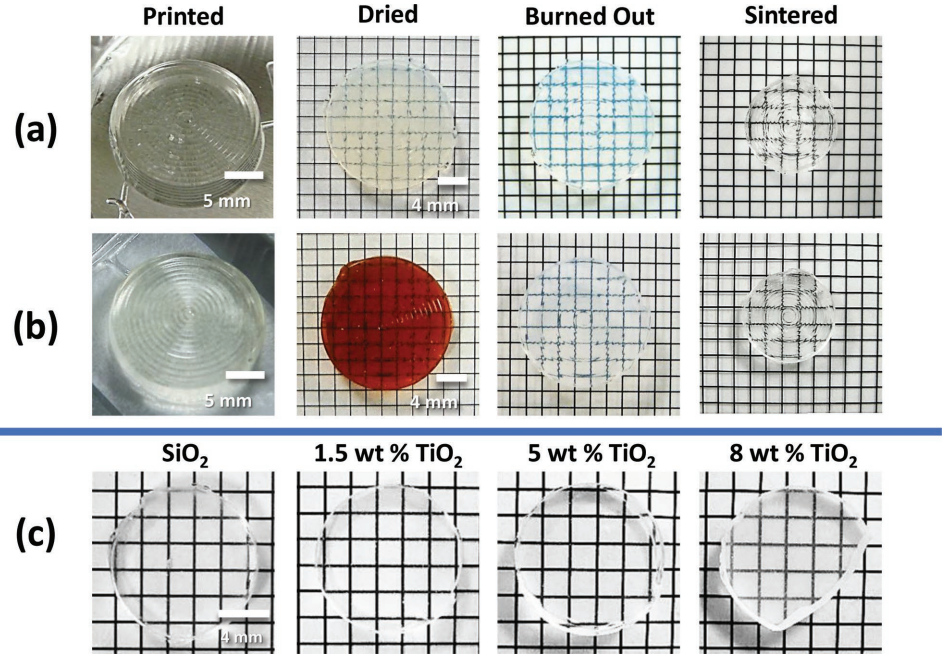

Figure 4. DIW sol–gel and glass components at various stages. a) A typical DIW SiO_2 part after: (1) printing; (2) drying at 100 °C for 5 d; (3) burn out at 500 °C for 2 h; (4) sintering at 1150 °C for 2 h. b) A typical DIW 1.5 wt% TiO_2 part after: (1) printing; (2) drying at 100 °C for 5 d; (3) burn out at 500 °C for 2 h; (4) sintering at 1150 °C for 2 h (unpolished). c) Typical polished, fully dense, transparent SiO_2, 1.5, 5, and 8 wt% TiO_2 DIW glasses.

X-ray diffraction (XRD) of the fully dense glasses provides insight into structural phase analysis to understand SiO_2 and TiO_2 phase segregation. Finally, ^{29}Si magic angle spinning (MAS) nuclear magnetic resonance (NMR) spectroscopy of the fully dense glasses provides insight into the network structure through Q-species analysis.

2.2.1. Chemical Conversion of Sol–Gel Feedstocks

Figure 5a shows FTIR transmission spectra for SiO_2, 1.5, 5, and 8 wt% TiO_2 nanoparticle feedstocks after heat treatment at 100 and 500 °C. Frequencies of interest are denoted with dashed gray-blue lines. Generally, frequencies or vibrational motions of interest can be grouped into three clusters: organic, surface/SiO_2–TiO_2 cross-linked, and bulk-network species.

The key organic species corresponds to the band at 1460 cm^{-1}, an asymmetric methyl ($-CH_3$) bend ($\delta_a(CH_3)$) indicative of residual alkoxide groups from the TEOS and TIP precursors.[37,38] At 100 °C, a very subtle band indicates that an alkoxide residue remains in all samples. This is likely from residual, unhydrolyzed alkoxide groups on the SiO_2 and TiO_2 surfaces. At 500 °C, the $\delta_a(CH_3)$ band is no longer present, indicative of complete organic removal.

The band at about 950 cm^{-1} is a convolution of two relevant surface species; free silanol (ν(Si—OH)) and cross-linked (ν(Si—O—Ti)) moieties and the broad band about 600 cm^{-1} represents various Si and Ti dangling surface groups, specifically, (δ(Ti—O^-)) and (δ(Si—O^-)).[39–41] For SiO_2, a strong 950 cm^{-1} band at 100 °C can be attributed to ν(Si—OH), as Ti—O—Si functional groups are not expected. At 500 °C, this band disappears, indicative of SiO_2 particle dehydration via polycondensation and network densification. For 1.5 wt% TiO_2, this band remains relatively constant between 100 and 500 °C. This can be interpreted as a result of a complete reaction between TIP and free surface silanols on the core SiO_2 particle, leaving cross-linked Si—O—Ti structures which remain after heat treatment to 500 °C.[42] In both 5 and 8 wt% TiO_2, an increase in the intensity of the 950 cm^{-1} band is observed between heat treatment at 100 and 500 °C, suggesting that additional Si—O—Ti bonds form. This is likely a result of polycondensation between the core SiO_2 particle and proximal TiO_2 particles. For the broad band about 600 cm^{-1}, generally there is a loss of these surface groups at 500 °C, indicative of network growth and densification via polycondensation in all of the samples.

Regarding bulk-network species, the broad bands at 1000–1300 cm^{-1} are symmetric and asymmetric siloxane (Si—O—Si) stretches ($\nu_{a,s}$(Si—O—Si)), which for network structures are attributed to the longitudinal and transverse (TO) optical phonon modes.[41] Since these are nanoparticle structures from molecular precursors, these bands are very broad due to an ensemble of siloxane structures (macromolecular, surface, bulk, etc.). The band at 810 cm^{-1} is representative of a siloxane stretch, which in networks is the TO_2 mode.[41] In macromolecular structures, this region also includes tetrahedrally coordinated silica (SiO_4) ring species.[37] For SiO_2, the broad siloxane bands narrow significantly at 500 °C, especially ν_a(Si—O—Si) at 1105 cm^{-1}. This narrowing, accompanied by a shift, is indicative of SiO_2 nanoparticle network densification.[38] This observation is confirmed by the band at 810 cm^{-1} which decreases with thermal processing to 500 °C, suggesting a decrease in the SiO_4 ring species, and is also consistent with network growth in the SiO_2 particles a result of thermal treatment. The structural

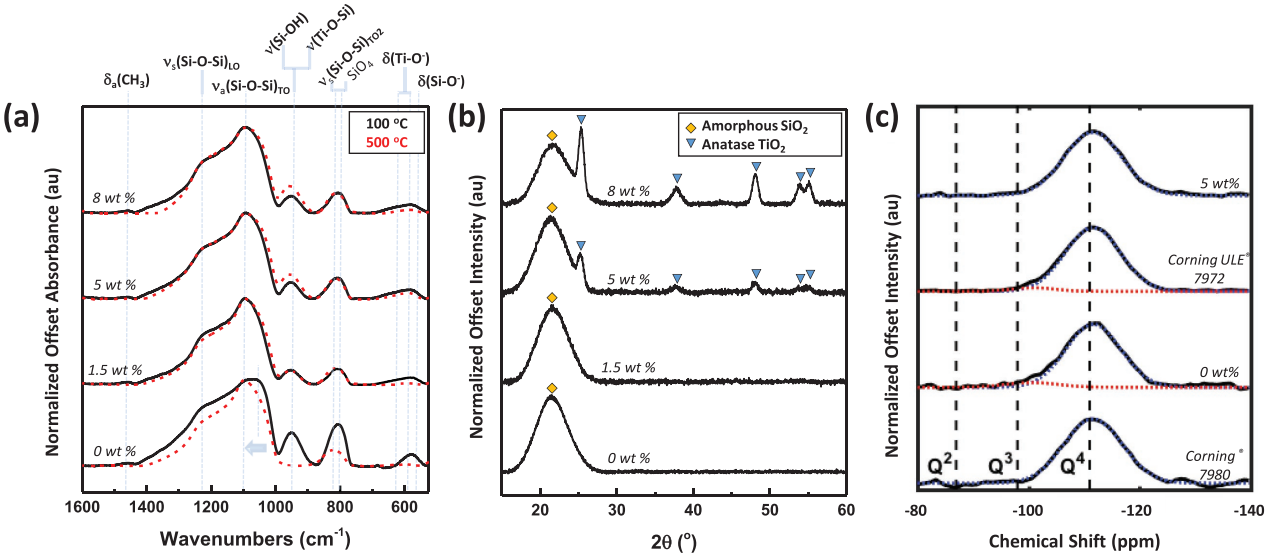

Figure 5. Chemical and structural evolution of DIW feedstocks to 3D printed glasses. a) FTIR transmission spectra of sol–gel feedstocks after heating to 100 and 500 °C. b) XRD patterns for DIW printed glasses. c) ^{29}Si MAS NMR of DIW SiO_2 and 5 wt% TiO_2 glasses compared with commercial silica and silica–titania glasses (Corning 7980 and ULE 7972, respectively). Solid lines represent the spectra; red and blue dashed lines represent deconvolutions of Q^4 and Q^3 species, respectively.

bands remain relatively consistent across core–shell SiO_2–TiO_2 particles, suggesting that the SiO_2 core structure forms a denser network after functionalization with TiO_2 without the need for additional heat treatment.

2.2.2. Phase Analysis of DIW Glasses

Figure 5b shows XRD results for each of the printed glasses after sintering. Results confirm that the SiO_2 and 1.5 wt% TiO_2 retain an amorphous structure after sintering. The 5 and 8 wt% TiO_2 printed parts show the emergence of anatase phase TiO_2 diffraction pattern. In general, the anatase peaks are broad and weak, suggesting a low concentration of TiO_2 nanocrystallite domains. Nanocrystallite size was determined by the Scherrer equation, by fitting the primary peak of anatase TiO_2 (25.34°). The TiO_2 nanocrystallite domains were determined to be 8.3 ± 1.4 and 11.4 ± 0.5 nm for 5 and 8 wt% TiO_2, respectively.[43,44] This observation is consistent with DLS and TEM findings for 5 wt% TiO_2 (cf. Figure 2), which suggested that the TiO_2 domains are on the order of 2–5 nm in diameter atop the SiO_2 core surface.

2.2.3. Silica Network Characterization of DIW Glasses

Figure 5c shows solid-state ^{29}Si MAS NMR Q-species analysis to compare the silica network of DIW printed glasses with commercial optical quality glasses. DIW sol–gel derived SiO_2 and 5 wt% TiO_2 glasses were compared directly with commercial optical quality fused silica (Corning 7980) and silica–titania glass (Corning ULE 7972), respectively. All samples are composed of predominately Q^4 species, indicative of a fully dense silica network. A slight shoulder in the Q^3 position is apparent in both the DIW silica and the commercial silica–titania glasses, hinting at the presence of silica dangling bonds in these materials. However, this feature is very small in both the samples and accounts for less than 5% of the total network structure. Overall, Q-species analysis indicates that DIW SiO_2 and SiO_2–TiO_2 glasses are fully dense (Q^4) networks and compared directly with commercial optical quality glasses.

2.3. Optical Characterization and Performance

While the structure of DIW glasses has been shown to be comparable to conventionally prepared commercial counterparts, it is important to assess their optical performance. **Figure 6** includes UV–vis transmission, optical dispersion, and optical homogeneity results for DIW printed glasses to compare directly with commercial materials. Furthermore, **Table 1** provides a side-by-side comparison of several key properties to directly compare commercial SiO_2 and SiO_2–TiO_2 with DIW analogs.

Figure 6a shows UV–vis transmission spectra for Corning 7980, Corning ULE 7972, and polished DIW:SiO_2, 1.5, 5, and 8 wt% TiO_2 over 200–1100 nm. Upon inspection, the general shape for the DIW SiO_2 optical transmission compares well with Corning 7980, transmitting greater than 80% across the spectrum. Corning ULE 7972 exhibits an absorption band edge at 275 nm, which is attributed to amorphous TiO_2. Comparably, 1.5 wt% TiO_2 DIW glass exhibits a band edge at 260 nm, which can also be attributed to amorphous TiO_2. Since 5 and 8 wt% TiO_2 glasses contain anatase TiO_2 domains, the band edge shifts to 365 nm.[45] Figure 6b shows the optical dispersion curves for same suite of samples. DIW SiO_2 compares directly with its commercial analog. This is quantitatively confirmed in the recovered Abbe numbers (V_d), shown in Table 1. As expected, glasses

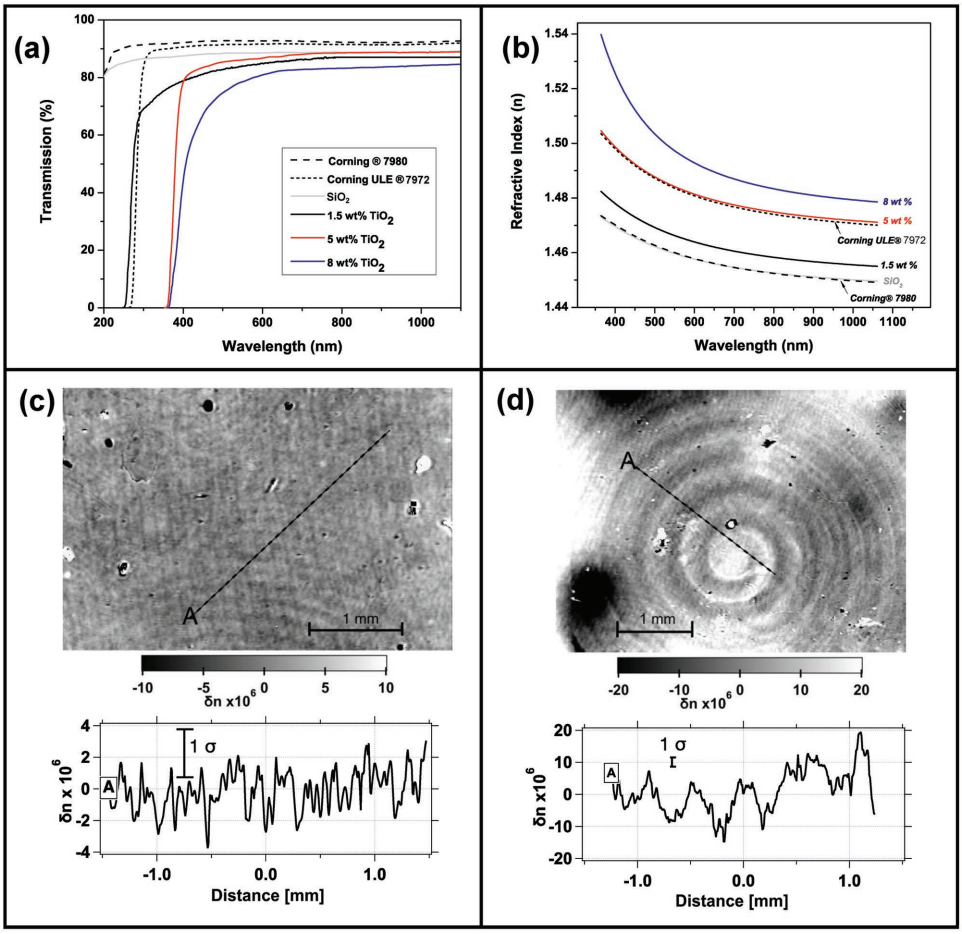

Figure 6. Optical characterization of polished DIW, 3D printed glasses. a) UV–vis optical transmission spectra. b) Optical dispersion curves. c,d) Refractive index variation images for DIW SiO_2 and 5 wt% TiO_2 glasses, respectively. Typical line profiles are given below to demonstrate relative standard deviation and peak-to-valley variations. A typical error bar is given on the line profiles to illustrate estimated 1σ in the thickness-averaged fractional refractive index variation at each pixel.

with increasing TiO_2 content exhibit an increase in n, with 8 wt% TiO_2 exhibiting the highest n values and the greatest dispersion. The increase in dispersion with TiO_2 content is shown to be in good agreement with absorption edges shown in Figure 6a. However, the relative n increase noted in DIW TiO_2 containing glasses contrasts with existing literature.[46] Elemental analysis by laser ablation (LA) inductively coupled plasma mass spectrometry (ICP-MS) confirms (shown in Figure S2 in the Supporting Information) that the actual TiO_2 content is 7.4 ± 0.2 wt% for ULE, 2.6 ± 0.1 wt% for DIW 1.5 wt% TiO_2, 6.0 ± 0.2 wt% for DIW 5 wt% TiO_2, and 8.5 ± 0.2 wt% for DIW 8 wt% TiO_2. The observed 0.5–1 wt% concentration increase over the DIW glass design targets is attributed to a loss in unreacted TEOS/SiO_2 during solvent exchange. Additionally, the presence of crystalline TiO_2 may provide refractive index enhancement in DIW 5 and 8 wt% TiO_2 glasses beyond what would be expected based on the TiO_2 concentration alone. Thus, n values and dispersion for DIW SiO_2–TiO_2 glasses are higher than expected literature values.

A major concern with developing 3D-printed glasses is that defects will be created at interfaces which will translate into optical path length or refractive index inhomogeneity. Figure 6c,d presents typical index homogeneity images, measured through the bulk of the polished DIW SiO_2 and 5 wt% TiO_2 glasses, respectively. Samples were polished on both faces to remove the effect of surface topography. Figure 6c shows that the DIW SiO_2 exhibits no noticeable inhomogeneity as a result of the print pattern. Some defects are apparent, but these can be attributed to bulk contaminants or voids. The line profile drawn on the top image shows that the relative variation is on the order of 7 ppm peak-to-valley with $1\sigma = 1.2$ ppm. These values are within the realm of the Corning 7980 standard (cf. Table 1) and are evidence that optical quality, homogeneous DIW fused silica glass is attainable. Figure 6d shows an index homogeneity image for 5 wt% TiO_2 with the characteristic spiral build pattern clearly represented. However, the 20 ppm peak-to-valley variation shown in the extracted line profile is still within the acceptable limits of optical glass, proving that 3D printed optical quality SiO_2–TiO_2 glass is also attainable. We are currently investigating the source of the higher index variability for the 5% TiO_2 glass relative to the silica-only glass.

Table 1 provides a complete list of the physical, optical, and structural properties for the DIW SiO_2 and 5 wt% TiO_2 glasses

Table 1. Properties of commercial SiO_2 and SiO_2–TiO_2 glasses and DIW analogs.

Property	Corning 7980	DIW SiO_2 glass	Corning ULE 7972	DIW 5 wt% TiO_2 glass
TiO_2 [wt%]	0	0	7.4 ± 0.2[a)]	6.0 ± 0.2[a)]
Density [g cc^{-1}]	2.2	2.2	2.2	2.2
n_{532nm}	1.461	1.461	1.486	1.483
Abbe (V_d)	62.8	59.4	47.6	48.6
RMS μ-roughness [nm]	0.3–0.4	0.3–0.6	0.3–0.4	0.3–0.6
Index homogeneity [ppm]	0.5–5	1.2	NR	10–20
XRD	a-SiO_2	a-SiO_2	a-SiO_2	a-SiO_2 and 8.3 ± 1.4 nm TiO_2
^{29}Si MAS NMR	Q^4 only	Q^4 only	Q^4 only	Q^4 only
−OH [wt%] ($A_{3680cm-1}$)	0.009	0.069	0.005	0.069

[a)]Denotes value determined by LA-ICP-MS; a-SiO_2 used to represent amorphous SiO_2.

alongside the commercial counterparts. Additional measured specifications include: density, achievable microroughness (μ-roughness) after convergent polishing,[47] and hydroxyl content. First, all DIW glasses were determined to be full density by Archimedes' method, thus, compared directly with commercial materials. Second, generally, DIW glasses can be polished to surfaces with root mean square (RMS) μ-roughnesses comparable to those achievable with the commercial glasses. Third, hydroxyl content is approximately an order of magnitude greater for DIW glasses. This is likely the cause of the slight Q^3 shoulder apparent by NMR (cf. Figure 5c). As a result, there is room for improvements to be made in the sintering process. One solution being explored is the implementation of a vacuum sintering process.[26] Finally, to date, the primary application of SiO_2–TiO_2 glass has been for use as ultralow coefficient of thermal expansion (CTE) materials in various optical applications. CTE measurements for the DIW glasses and commercial fused silica and ULE glasses are available in Figure S3 (Supporting Information). All of the printed glasses performed similarly to the commercial fused silica and ULE glasses, with average CTE ranging from 0 to 30 ppm $°C^{-1}$. Unfortunately, the measurement technique did not provide enough precision to permit differentiation between the various TiO_2 concentrations.

More broadly, sol–gel derived DIW glasses represent an initial breakthrough for a potentially paradigm shifting technology. These findings demonstrate in a rigorous manner that high quality, conventional optical materials can be prepared by unconventional means. Ongoing efforts seek to validate that sol–gel derived DIW glasses can surpass conventional methods for fabricating unconventional optics and optical components. However, the potential for one-pot, sol–gel derived feedstocks for 3D printing extends far beyond optical applications and could offer advantages for applications demanding inorganic scaffolds with unique chemistries, such as for catalysis and separations.

3. Conclusions

Optical quality silica and silica–titania glasses have been prepared from sol–gel derived SiO_2, and SiO_2–TiO_2 feedstocks by DIW 3D printing. Printable inks were obtained by a simple one-pot method which yielded viscous, shear-thinning colloidal suspensions, or "inks" with tuned rheology. The as-prepared inks were then printed into monoliths, dried, and sintered under optimized conditions to ensure complete organic removal and uniform densification, resulting in optical quality glasses. Chemical and structural evolutions were confirmed by several techniques, and sol–gel derived DIW glasses compared well with commercial counterparts. Optical quality assessments reveal that DIW glasses exhibit densities, dispersion, μ-roughness, index homogeneity, and thermal expansion properties comparable to those of their commercial counterparts.

This one-pot, sol–gel approach to ink formulation is expected to greatly expand the range of accessible feedstock materials suitable for glass 3D printing, as the sol–gel chemistry can be readily tuned for preparing a wide range of glass-forming metal oxide feedstock particles. In addition, the method provides multiple avenues by which to tune and control ink rheology. Further, because these inks are compatible with DIW technology, which offers numerous advantages for building components with unique geometries, the method is anticipated to enable additively manufactured optical glasses and functional ceramics in compositional and geometrical configurations inaccessible by conventional fabrication methods.

4. Experimental Section

Sample Preparation—Reagents: EtOH (Pharmco-AAPER, 200 Proof ACS/USP Grade, ≥99.5%)), concentrated ammonium hydroxide (NH_4OH) (Sigma-Aldrich, 28 wt% in H_2O, ≥99.99%), TEOS (ATMI, ultrapure double distilled), TIP (Sigma-Aldrich, ≥97%), deionized water, PC (Sigma-Aldrich, anhydrous, 99.7%), TG (Sigma-Aldrich, ≥99%), MEEAA (Sigma-Aldrich, technical grade), 1-hexanol (Sigma-Aldrich, reagent grade, 98%).

Sample Preparation—Sol–Gel Nanoparticle Growth: Silica sols were prepared by mixing EtOH, NH_3 (from $NH_4OH_{(aq)}$), H_2O, and TEOS in a 16.42:0.14:2.88:1.00 mole ratio. In a typical batch of silica sol (9.5 g SiO_2, 5.6 wt% solids) (sol A) was prepared by mixing 152 mL of EtOH, 1.50 mL of concentrated NH_4OH, 7.24 mL of H_2O, 35.36 mL of TEOS in a round bottom flask. The sol was then aged at ambient for a minimum of 5 d.

Silica–titania sols were prepared by reacting the surface of the silica particle with TIP. To control reactivity, TIP was introduced to sol A in

a 10 vol% TIP:EtOH solution. In a typical silica–titania batch with a 1.5 wt% TiO_2 total solids (0.14 g TiO_2) (sol B), a 0.60 mL TIP/5.40 mL EtOH solution was added to sol A. In a typical silica–titania batch with 5 wt% TiO_2 total solids (0.5 g TiO_2) (sol C), a 1.87 mL TIP/16.92 mL EtOH solution was added dropwise to sol A. In a typical silica–titania batch with 8 wt% TiO_2 total solids (0.82 g TiO_2) (sol D), a 3.10 mL TIP/27.90 mL EtOH solution was added dropwise to sol A. For sols B, C, and D, the resulting mixtures were then heated at 55 ± 2 °C with continuous stirring until the pH of the solution was neutral; typically, 2–3 d. Finally, upon completion, sols were vacuum filtered using a Büchner funnel (Whatman filter paper, Grade 6) to remove agglomerates before solvent exchange.

Sample Preparation—Glass Ink Formulation: Inks were prepared by a one-pot solvent exchange method. Low vapor pressure ink solvents were added to the original sol, and EtOH and H_2O were subsequently removed by rotary vacuum evaporation and confirmed gravimetrically (±3%). The resulting ink was scraped from the flask, syringe filtered through a 100 µm stainless mesh to remove any agglomerates and/or contaminants introduced during exchange, then mixed using a planetary centrifugal mixer (Thinky-USA) for 30 s at 2000 RPM.

Silica inks were prepared from sol A for a final composition of: 33.5 ± 0.2 wt% or 20.0 ± 0.1 vol% SiO_2 solids, 33.8 ± 0.3 wt% PC, 30.5 ± 0.3 wt% TG, 0.8 ± 0.2 wt% 1-hexanol, and 0.5 ± 0.1 wt% MEEAA. A typical batch contained: 9.63 g PC, 8.75 g TG, 0.34 g 1-hexanol, and 0.17 g MEEAA.

Silica–titania inks were prepared from sols B, C, and D for a final composition of: 33.5 ± 0.2 wt% or 20.0 ± 0.1 vol% SiO_2–TiO_2 solids, 36.3 ± 0.1 wt% PC, 30.3 ± 0.1 wt% TG. A typical batch from sol B contained 10.50 g PC and 8.75 g TG. A typical batch from sol C contained 10.85 g PC and 9.05 g TG.

Sample Preparation—Glass Ink 3D Printing: Inks were loaded into 30 cm^3 syringe barrels (Nordson EFD), then centrifuged at 4000 RPM for 3 min. Next, the ink-loaded syringes were installed in a fixed holder suspended above a three-axis rotary micropositioning stage (Aerotech). A constant displacement drive delivered the ink through a 610 µm nozzle at a linear feed rate of 10 mm s^{-1} onto a flat substrate.

Sample Preparation—Glass Thermal Processing: The thermal profile for drying, organic removal, and sintering is given in Figure S1 (Supporting Information). Briefly, printed silica and silica–titania monolithic preforms (low density structures) were ramped at 3 °C h^{-1} to 75 °C and held constant for 48 h. At this point, the samples were released from the substrate to prevent stress formation due to print-substrate adhesion. Afterward, the unconstrained preforms were ramped at 3 °C h^{-1} to 100 °C and held constant for 100 h, where the majority of solvent was removed. Next, the preforms were ramped at 10 °C h^{-1} to 500 °C and held for 2 h to eliminate any remaining organic residue. Last, the inorganic preforms were ramped at 60 °C h^{-1} to 1150 °C, held for 2 h, and then cooled down to room temperature, yielding sintered, full density glasses. Note: all heat treatments were performed in air.

Sample Preparation—Glass Polishing: 3D-printed glass parts were first ground using 15T Microgrit aluminum oxide grinding compound (Universal Photonics) on a rotating lap under manual load to reduce microscale surface texture, resulting in ≈100 µm of material removal. Then, the ground parts were polished on both sides under manually applied load over a polyurethane pad (MHN Pad, Eminess Technologies) rotating at 20 rpm, using stabilized Hastilite PO (Universal Photonics) ceria polishing slurry.[48] Parts were polished until the μ-roughness across the sample was less than ≈1 nm RMS. For comparison, typical μ-roughness is reported for 2 in. rounds of the commercial glasses (Corning 7980 and Corning ULE 7972) polished on pads with stabilized Hastilite by the convergent polishing method.[49,50]

Material Characterization—Glass Ink Rheology Characterization: Rotational rheology measurements were performed on a TA Instruments DHR-1 rheometer, using a 25 mm stainless steel parallel plate setup. The temperature of the Peltier plate was kept at 23 °C to match ambient conditions during printing. All measurements were done with a sample thickness (geometry gap) of 500 µm. Ink viscosities were measured at shear rates ranging from 0.01 to 100 s^{-1}. Oscillatory measurements of the elastic and viscous moduli were performed at a constant frequency of 1 Hz.

Material Characterization—Chemical and Structural Determination: Transmission FTIR spectroscopy measurements were acquired with a Thermo-Fisher Nicolet iS10 spectrometer. Samples were prepared by drying each sol on pristine KBr windows (International Crystal Laboratories) at 100 and 500 °C temperature for 1 h. XRD measurements were acquired with a Bruker D8 Advance X-ray diffractometer equipped with Cu anode operated at 40 kV and 40 mA. Samples were ground using an agate mortar and pestle and deposited onto a zero diffraction Si sample holder for analysis.

DLS measurements were acquired with a Nanobrook 90Plus (Brookhaven Instruments Corp.) particle size analyzer. For each measurement, 100 µL of as-prepared sol was diluted in 2 mL of EtOH and subsequently measured in triplicate. Reported values are given as mean and standard deviation (for $n \geq 3$ samples).

Electron images were acquired with a FEI Titan TEM operating at an accelerating voltage of 300 kV. Samples were prepared by drop casting 5 µL of as-prepared sample sol diluted 100-fold with EtOH onto an ultrathin carbon film on lacy carbon support film Cu mesh (Ted Pella) and allowed to dry under ambient conditions.

Solid state ^{29}Si MAS NMR experiments were carried out on a 300 MHz (7.5 T) Tecmag Apollo with a 7.5 mm Chemagnetics cross polarization (CP) MAS probe tuned to 59.8 MHz. A 30° tip angle of 4 µs was applied, followed by data acquisition without high-powered proton decoupling. Average spinning speeds were 4–5 kHz and the experimental delay was 996 s. Chemical shifts were referenced to kaolinite at –91.5 ppm. Density values were determined by Archimedes method (GAOTek).

Material Characterization—Optical Characterization: UV–vis transmission spectra were acquired on a Shimadzu UV-1601 PC spectrophotometer. DIW glass samples were ≈2 mm thick and commercial standards were 0.5 mm thick. Refractive indices of the bulk commercial and DIW glasses were measured using a Metricon model 2010 prism coupler at 377, 532, and 1061 nm. Dispersion values were calculated from a Cauchy fit of the measured refractive index data set. All optical measurements were acquired with polished samples.

Material Characterization—Hydroxyl Measurement: Transmission FTIR spectra were acquired for both commercial and 3D-printed silica and silica–titania glasses on samples with thicknesses ranging from 0.5 to 2 mm. Absorbance at 3676 cm^{-1} was extracted from each spectra and then converted to [—OH] using an absorption coefficient of 181 mol cm^{-1} L^{-1}, as described in a previously reported method.[51] All hydroxyl measurements were acquired with polished samples.

Material Characterization—RMS μ-Roughness Measurement: Surface μ-roughnesses of polished 3D-printed glass samples were measured using a WYKO NT3300 white light interferometer. Values are reported as typical RMS deviations measured over multiple 0.9 mm × 1.2 mm fields of view.

Material Characterization—Index Homogeneity Measurement: Visible light (532 nm) interferometry was performed to measure lateral variations in the thickness-averaged refractive index of the 3D-printed samples. Transmitted optical path difference (OPD) was mapped through the sample using a small-aperture special-purpose phase shifting interferometer that has a lateral resolution of about 12 µm. This OPD is the sum of contributions from thickness variations and from bulk variations in the refractive index. The thickness contribution to the OPD is removed by separately measuring height variations in both surfaces using a commercial interferometric surface profiler (WYKO model NT8900). Spatial registration of the surface maps with the transmission OPD map was aided by placing small ink fiducial marks on both surfaces. Finally, thickness-averaged refractive index variation was calculated by dividing the resulting surface-corrected OPD map by the nominal sample thickness. Based on similar data taken on a superpolished fused silica reference flat, it was estimated that for spatial scales ranging from 10 µm to 1 mm, this method gives refractive index homogeneity data with a standard deviation of about 3×10^{-6}. All index homogeneity measurements were acquired with polished samples.

Supporting Information

Supporting Information is available from the Wiley Online Library or from the author.

Acknowledgements

The authors would like to thank Taylor Bryson for performing the CTE measurements and Paul Ehrmann for collecting DLS data. EAG Laboratories (Liverpool, NY) performed the ICP-MS analysis. This work was performed under the auspices of the U.S. Department of Energy by Lawrence Livermore National Laboratory under Contract DE-AC52-07NA27344 within the LDRD program 16-SI-003, LLNL-JRNL-737841.

Conflict of Interest

The authors declare no conflict of interest.

Keywords

3D printing, direct ink writing, glass, optics, sol–gel

Received: November 8, 2017
Revised: December 15, 2017
Published online:

[1] N. P. Bansal, R. H. Doremus, *Handbook of Glass Properties*, Elsevier, New Delhi, India **2006**.
[2] J. E. Shelby, *Introduction to Glass Science and Technology*, Royal Society of Chemistry, Cambridge, UK **2009**.
[3] D. L. Evans, *J. Am. Ceram. Soc.* **1970**, *53*, 418.
[4] M. Kawachi, M. Yasu, T. Edahiro, *Electron. Lett.* **1983**, *19*, 583.
[5] G. Brusatin, M. Guglielmi, P. Innocenzi, A. Martucci, G. Battaglin, S. Pelli, G. Righini, *J. Non-Cryst. Solids* **1997**, *220*, 202.
[6] K. Shingyouchi, S. Konishi, *Appl. Opt.* **1990**, *29*, 4061.
[7] B. Zhang, M. Montgomery, M. D. Chamberlain, S. Ogawa, A. Korolj, A. Pahnke, L. A. Wells, S. Masse, J. Kim, L. Reis, A. Momen, S. S. Nunes, A. R. Wheeler, K. Nanthakumar, G. Keller, M. V Sefton, M. Radisic, *Nat. Mater.* **2016**, *15*, 669.
[8] J. U. Lind, T. A. Busbee, A. D. Valentine, F. S. Pasqualini, H. Yuan, M. Yadid, S.-J. Park, A. Kotikian, A. P. Nesmith, P. H. Campbell, J. J. Vlassak, J. A. Lewis, K. K. Parker, *Nat. Mater.* **2017**, *16*, 303.
[9] J. P. Lewicki, J. N. Rodriguez, C. Zhu, M. A. Worsley, A. S. Wu, Y. Kanarska, J. D. Horn, E. B. Duoss, J. M. Ortega, W. Elmer, R. Hensleigh, R. A. Fellini, M. J. King, *Sci. Rep.* **2017**, *7*, 43401.
[10] J. R. Tumbleston, D. Shirvanyants, N. Ermoshkin, R. Januszewicz, A. R. Johnson, D. Kelly, K. Chen, R. Pinschmidt, J. P. Rolland, A. Ermoshkin, E. T. Samulski, J. M. DeSimone, *Science* **2015**, *347*, 1349.
[11] W. E. Frazier, *J. Mater. Eng. Perform.* **2014**, *23*, 1917.
[12] C. Ladd, J. H. So, J. Muth, M. D. Dickey, *Adv. Mater.* **2013**, *25*, 5081.
[13] J. Bauer, A. Schroer, R. Schwaiger, O. Kraft, *Nat. Mater.* **2016**, *15*, 438.
[14] G. Marchelli, R. Prabhakar, D. Storti, M. Ganter, *Rapid Prototyping J.* **2011**, *17*, 187.
[15] J. Luo, H. Pan, E. C. Kinzel, *J. Manuf. Sci. Eng.* **2014**, *136*, 1.
[16] J. Luo, L. Gilbert, C. Qu, J. Wilson, D. Bristow, R. Landers, E. Kinzel, in *Proc. ASME 2015 Int. Manufacturing Science and Engineering Conf.* Vol. *1*, ASME, Charlotte, NC, USA **2015**, p. V001T02A108, https://doi.org/10.1115/MSEC2015-9377.
[17] J. Luo, L. J. Gilbert, C. Qu, R. G. Landers, D. A. Bristow, E. C. Kinzel, *J. Manuf. Sci. Eng.* **2017**, *139*, 61006.
[18] F. Kotz, K. Arnold, W. Bauer, D. Schild, N. Keller, K. Sachsenheimer, T. M. Nargang, C. Richter, D. Helmer, B. E. Rapp, *Nature* **2017**, *544*, 337.
[19] F. Kotz, K. Plewa, W. Bauer, N. Schneider, N. Keller, T. Nargang, D. Helmer, K. Sachsenheimer, M. Schäfer, M. Worgull, C. Greiner, C. Richter, B. E. Rapp, *Adv. Mater.* **2016**, *28*, 4646.
[20] D. T. Nguyen, C. Meyers, T. D. Yee, N. A. Dudukovic, J. F. Destino, C. Zhu, E. B. Duoss, T. F. Baumann, T. Suratwala, J. E. Smay, R. Dylla-Spears, *Adv. Mater.* **2017**, *29*, 1701181.
[21] I. K. Jones, Z. M. Seeley, N. J. Cherepy, E. B. Duoss, S. A. Payne, *Opt. Mater.*, **2018**, *75*, 19.
[22] K. M. R. Kallury, P. M. Macdonald, M. Thompson, *Langmuir* **1994**, *10*, 492.
[23] R. Merget, T. Bauer, R. Breitstadt, T. Bruening, *Arch. Toxicol.* **2002**, *75*, 625.
[24] E. B. Duoss, M. Twardowski, J. A. Lewis, *Adv. Mater.* **2007**, *19*, 3485.
[25] G. H. Bogush, M. A. Tracy, C. F. I. Zukoski, *J. Non-Cryst. Solids* **1988**, *104*, 95.
[26] L. T. Zhuravlev, *Colloids Surf., A* **2000**, *173*, 1.
[27] C. J. Brinker, G. W. Scherer, *Sol-Gel Science: The Physics and Chemistry of Sol-Gel Processing*, Academic Press, Boston, MA, USA **1990**.
[28] C. J. Brinker, M. S. Harrington, *Sol. Energy Mater.* **1981**, *5*, 159.
[29] T. I. Suratwala, M. L. Hanna, E. L. Miller, P. K. Whitman, I. M. Thomas, P. R. Ehrmann, R. S. Maxwell, A. K. Burnham, *J. Non-Cryst. Solids* **2003**, *316*, 349.
[30] M. A. Aegerter, *Sol-Gel Technologies for Glass Producers and Users*, Springer, New York, NY, USA **2011**.
[31] S. Son, S. H. Hwang, C. Kim, J. Y. Yun, J. Jang, *ACS Appl. Mater. Interfaces* **2013**, *5*, 4815.
[32] X. Li, J. He, *ACS Appl. Mater. Interfaces* **2013**, *5*, 5282.
[33] S. R. Raghavan, H. J. Walls, S. A. Khan, *Langmuir* **2000**, *16*, 7920.
[34] J. Mewis, N. J. Wagner, *Colloidal Suspension Rheology*, Cambridge University Press, New York, NY, USA **2012**.
[35] J. S. Weston, J. H. Harwell, B. P. Grady, *Soft Matter* **2017**, *13*, 6743.
[36] A. Leaustic, F. Babonneau, J. Livage, *Chem. Mater.* **1989**, *1*, 248.
[37] A. Bertoluzza, C. Fagnano, *J. Non-Cryst. Solids* **1982**, *48*, 117.
[38] A. Duran, C. Serna, V. Fornes, J. M. Fernandez Navarro, *J. Non-Cryst. Solids* **1986**, *82*, 69.
[39] A. Pirson, A. Mohsine, P. Marchot, B. Michaux, O. van Cantfort, J. P. Pirard, A. J. Lecloux, *J. Sol-Gel Sci. Technol.* **1995**, *4*, 179.
[40] M. Burgos, M. Langlet, *Thin Solid Films* **1999**, *349*, 19.
[41] A. M. Putz, M. V. Putz, *Int. J. Mol. Sci.* **2012**, *13*, 15925.
[42] M. C. Capel-Sanchez, G. Blanco-Brieva, J. M. Campos-Martin, M. P. De Frutos, W. Wen, J. A. Rodriguez, J. L. G. Fierro, *Langmuir* **2009**, *25*, 7148.
[43] A. Budnyk, A. Damin, S. Bordiga, A. Zecchina, *J. Phys. Chem. C* **2012**, *116*, 10064.
[44] H. Zhang, J. F. Banfield, *Chem. Mater.* **2005**, *17*, 3421.
[45] J. Pan, G. Liu, G. Q. Lu, H. M. Cheng, *Angew. Chem., Int. Ed.* **2011**, *50*, 2133.
[46] P. C. Schultz, *J. Am. Ceram. Soc.* **1976**, *59*, 214.
[47] T. Suratwala, R. Steele, M. Feit, R. Desjardin, D. Mason, *Int. J. Appl. Glass Sci.* **2012**, *3*, 14.
[48] R. Dylla-Spears, L. Wong, P. E. Miller, M. D. Feit, W. Steele, T. Suratwala, *Colloids Surf., A* **2014**, *447*, 32.
[49] T. Suratwala, M. Feit, W. Steele, L. Wong, N. Shen, R. Dylla-Spears, R. Desjardin, D. Mason, P. Geraghty, P. Miller, S. Baxamusa, *J. Am. Ceram. Soc.* **2014**, *97*, 81.
[50] T. Suratwala, personal communication.
[51] J. E. Shelby, J. Vitko, R. E. Benner, *J. Am. Ceram. Soc.* **1982**, *65*, 59.